ADVANCED FUNCTIONAL MATERIALS

Interfacial Polar-Bonding-Induced Multifunctionality of Nano-Silicon in Mesoporous Silica

By *Jung Y. Huang,* Jia M. Shieh,* Hao C. Kuo,* and *Ci L. Pan*

The optoelectronic response of a material governs its suitability for a wide range of applications, from photon detection to photovoltaic conversion. To conquer the material limitations and achieve improved optoelectronic responses, nanotechnology has been employed to arrange subunits with specific size-dependent quantum mechanical properties in a hierarchically organized structure. However, building a functional optoelectronic system from nano-objects remains a formidable challenge. In this paper, the fabrication of a new artificially engineered optoelectronic material by the preferential growth of silicon nanocrystals on the bottom of the pore-channels of mesoporous silica is reported. The nanocrystals form highly stable interface structures bonded on one side; these structure show strong electron–phonon coupling and a ferroelectric-like hysteretic switching property. A new class of multifunctional materials is realized by invoking a concept that employs semiconductor nanocrystals for optical sensing and utilizes interfacial polar layers to facilitate carrier transport and emulate ferroelectric-like switching.

1. Introduction

Optoelectronic response in a semiconductor material can be understood in terms of the generation of electron-hole pairs by photon absorption and the carrier transport that follows. The photoresponsivity of such materials in the lower energy side is usually limited by the fundamental bandgap of the semiconductor material used. To circumvent this limitation, nanotechnology has been employed to arrange subunits with specific size-dependent quantum mechanical properties in a hierarchically organized structure.[1] At the nanometer scale, the ratio of the number of atoms on the surface to that in the bulk increases rapidly, suggesting new functional devices could be made utilizing the interfacial properties of a nanostructured material.[2,3]

Two-terminal molecular junction can serve researchers an ideal device to peek into the carrier transport process at the single-molecule level. Electrons move through molecules under a voltage bias, showing the various degrees of coupling between the transporting charge and electric polarization,[4] which can originate from the molecular and environmental vibrational degrees of freedom. The vibronic coupling effects are strong when the time spent by the electron on the molecular bridge is long enough for the charge to interact with the nuclear dynamics. However, it remains a formidable task to assemble a functional optoelectronic system from molecular junctions.

A wide range of possible photonic applications with Si nanocrystals (*nc*-Si) has been reported.[5,6] Silicon nanocrystals can be synthesized in mesoporous silica (MS),[7] which is attractive for its self-assembling structures with extremely large internal surface areas and controllable nanoporous structures. In this paper, we show that the *nc*-Si/MS behaves like a three-dimensional array of nano-junctions with effects dominated by the *nc*-Si/MS interfaces and that this artificially designed material can surpass silicon crystal in terms of the optoelectronic response.

2. Results and Discussion

For material characterization, the test samples were prepared by spin coating a 100 nm thick MS nanotemplate layer on a *p*-type silicon substrate. The pore channels of MS can be clearly seen in the cross-sectional TEM image shown in Figure 1a. Si nanocrystals were thereafter synthesized in the MS templates by using the inductively coupled plasma chemical vapor deposition (ICP CVD) method.[8] A biased growth condition for preferential growth of *nc*-Si on the bottom of the pore-channels was created by applying an electrical power of 300 W at 300 kHz on the substrate during the synthesis of Si nanocrystals. Figure 1b shows a cross-sectional transmission electron microscopy (TEM) image of a typical *nc*-Si/MS film. The pore channels are no longer to be seen due to the contrast loss from the densification of silica during ICP CVD process. The distinct lattice fringes in the inset of Figure 1b indicate the highly crystalline quality of the Si nanocrystals. By examining the TEM image and analyzing the concentration profiles of specific atoms with secondary ion mass spectroscopy, we concluded that the average size and number density are ~4 nm and $\sim 2.5 \times 10^{18}\,\mathrm{cm}^{-3}$, respectively. Germanium nanocrystals with similar densities can also be obtained under identical sample preparation conditions, indicating similar growth mechanism for both silicon and germanium in the MS matrix.

[*] Prof. J. Y. Huang, Prof. J. M. Shieh, Prof. H. C. Kuo, Prof. C. L. Pan
Department of Photonics, National Chiao Tung University
1001 Ta-Hsueh Road, Hsinchu 30050 (Taiwan ROC)
E-mail: jyhuang@faculty.nctu.edu.tw
Prof. J. M. Shieh
National Nano Device Laboratories
26 Prosperity Road 1, Hsinchu 30078 (Taiwan ROC)
E-mail: jmshieh@ndl.org.tw

DOI: 10.1002/adfm.200801336

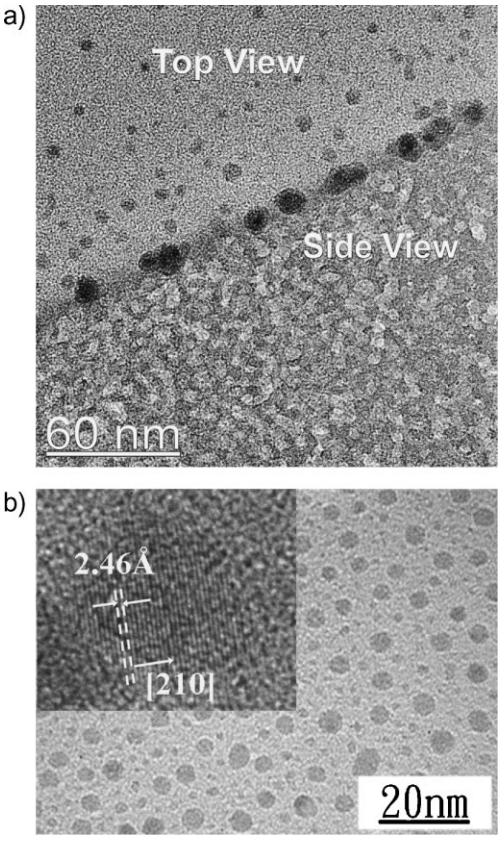

Figure 1. Cross-sectional TEM images of the pore channels and Si nanocrystals in mesoporous silica film: a) the pore channels (see the light-colored regions in the side view) of MS and b) *nc*-Si/MS; inset: the observed lattice fringes of silicon nanocrystals.

To demonstrate the optoelectronic response of Si nanocrystals bound to MS, we fabricated a two-terminal metal-oxide-silicon (MOS) photodetector,[9] with the structure of indium tin oxide (ITO) electrode/(*nc*-Si/MS)/*p*-Si (see the inset of Fig. 2). For comparison, the photoresponsivity of a typical *pn* diode (namely, ITO/*n*-Si/*p*-Si) is also included (the dashed line). The photoresponsivity of this reference device reversely biased at 5 V rises as wavelength increases from 300 to 900 nm, but the response is restricted to below 1.1 μm due to the limit of silicon fundamental bandgap. The measured photoresponse values for the ITO/(*nc*-Si/MS)/*p*-Si photodetector at the same bias voltage lie in the range of 0.4–1.0 A W^{-1} from 320 to 900 nm, which are significantly higher than those of the conventional Si photodetector. In the visible spectral region, this photodetector exhibits three resonant peaks at 422, 558 and 780 nm with photoresponse values 0.4, 0.7 and 0.9 A W^{-1}, respectively. The photodetector achieves an even higher value of 6 A W^{-1} at the wavelength of 944 nm. The appearance of resonant peaks suggests the optical response to be resonantly enhanced by the internal energy structure of the *nc*-Si/MS film used. We found that the optical response could reach 1.9 μm. Near-infrared photoresponsivity in nanostructured silicon has previously been observed with a Schottky barrier porous silicon photodetector.[10]

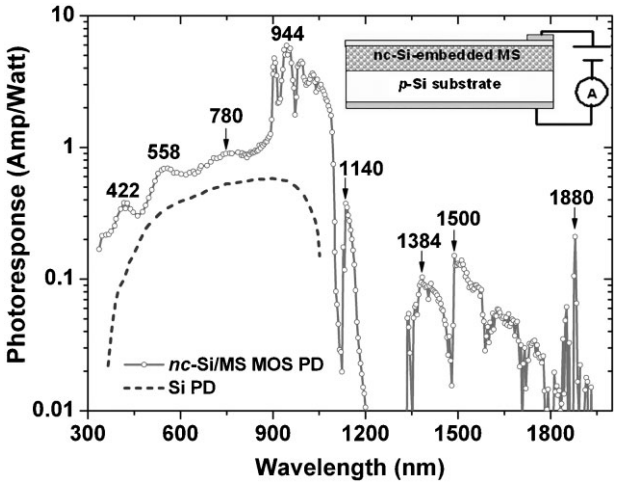

Figure 2. Photoresponse of *nc*-Si/MS. The optoelectronic signal (A/W) of a two-terminal device with indium tin oxide (ITO) electrode/(*nc*-Si/MS)/*p*-Si (inset) is plotted as a function of photon wavelength from 400 to 2000 nm (curve with symbols). For comparison, the photoresponsivity of a *pn* diode structure of ITO/*n*-Si/*p*-Si is included (dashed line).

To probe the mechanism leading to the enhanced photoresponse of *nc*-Si/MS, the photoluminescence (PL) spectrum of an as-grown *nc*-Si/MS film was measured and is presented in Figure 3a. It features a broad-band emission at $\lambda = 460$ nm. The spectral profile is complicated with shoulders, revealing the optical transitions involved originate from Si nanocrystals and nanoclusters, as shown in Figure 1b. After thermal annealing, the blue peak disappeared while a new luminescence band peaked around $\lambda \sim 700$ nm. The new peak wavelength depends on the size of the annealed Si nanocrystals. We attribute the blue PL emission to be from the interfacial states associated with defects of oxygen vacancy occurring in the MS matrix.[11] The embedded semiconductor nanocrystals play an important role by sensitizing the blue emission through the generation of more photoexcited carriers. These carriers are trapped in the interfacial oxygen defects and recombine to yield an increased PL intensity at 460 nm. Thermal annealing at 1 000 °C for 2 h effectively removes these defects and leads to the formation of isolated Si nanocrystals. Thus, the 700 nm PL peak originates from interband recombination of the isolated nanocrystals and reflects a quantum-confined size-effect.[12] The observed PL wavelength suggests the Si nanocrystals to be about 4–5 nm, in agreement with the TEM observation (Fig. 1b).

The annealing-induced change of bonding configurations can also be revealed with X-ray photoemission spectroscopy (XPS). However, to separate the nanocrystal signal from that of the mesosilica background, we synthesized *nc*-Ge instead of *nc*-Si in the MS, as Si and Ge nanocrystals are known to undergo similar growth process in the MS matrix. The spectral peak of the Ge-3*d* core level at 1 455 eV (the Ge−Ge bond geometry) and its chemical shift due to the existence of chemical bonds of Ge−O at 1 452 eV are clearly present in Figure 3b.[13] From the ratio of the areas of two deconvoluted peaks before and after thermal annealing, we confirmed that thermal annealing breaks the bonding of *nc*-Ge with the MS matrix and renders the embedded nanocrystals into isolated quantum dots.

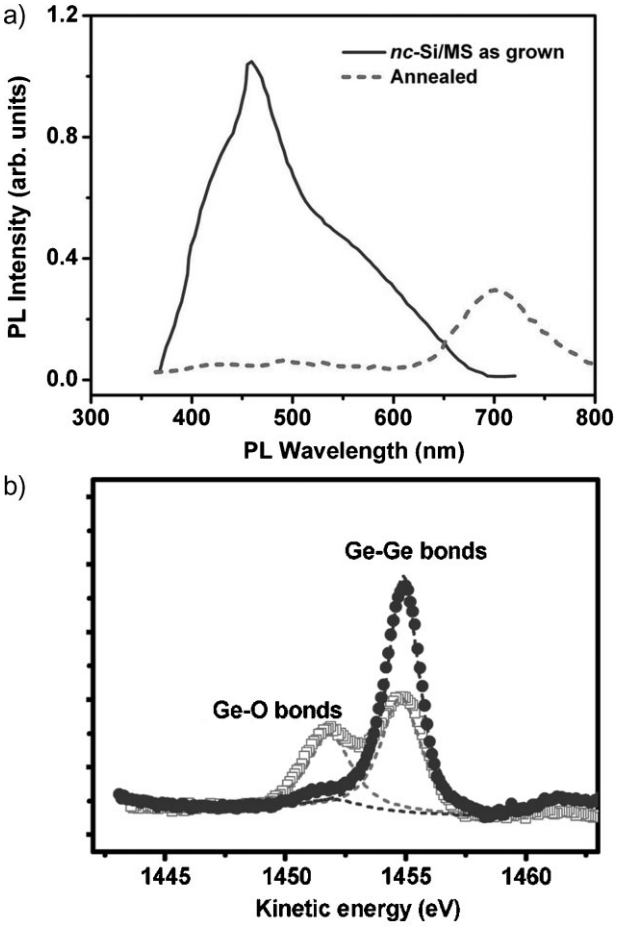

Figure 3. Spectroscopic data of the electronic structure of *nc*-Si/MS. a) Photoluminescence spectra of *nc*-Si/MS (solid curve) and the film thermally annealed at 1000°C for 2 h (dashed curve). b) XPS spectra of *nc*-Ge/MS before (open squares) and after (filled circles) annealing.

As shown above, interfacial bonding plays an important role in the optical response of *nc*-Si/MS. To advance our knowledge of the interfacial bonding nature of *nc*-Si/MS, we applied infrared-visible sum-frequency generation (IVSFG) vibrational spectroscopy to investigate the material. IVSFG belongs to the class of second-order nonlinear optical processes and is known for its unique capabilities in measuring surface sensitivity and molecular specificity.[14] The IVSFG intensity $I(\omega_s)$ generated from a sample with an effective surface susceptibility $\chi_s^{(2)}$ is given by $I(\omega_s) \propto \left|\hat{e}(\omega_s) \cdot \vec{\vec{\chi}}_s^{(2)} : \hat{e}(\omega_1)\hat{e}(\omega_2)\right|^2$, where $\hat{e}(\omega)$ is a unit vector describing the polarization of the optical field at frequency ω. The nonlinear optical susceptibility component $\chi_{ssp}^{(2)}$ for an *s*-polarized sum-frequency (SF) signal can be selected by using *s*-visible and *p*-infrared beams. Similarly, a polarization combination of *p*-SF signal, *p*-visible and *p*-infrared beams can be used to isolate the component of $\chi_{ppp}^{(2)}$. As the infrared frequency ω_1 is near resonance at ω_q, the IVSFG signal can be described by

$$I(\omega_s = \omega_1 + \omega_2) \propto \left|\chi_{NR} + \sum_q \frac{A_q}{\omega_1 - \omega_q + i\gamma_q}\right|^2 \quad (1)$$

with non-resonant susceptibility χ_{NR} and characteristic parameters of the resonances A_q, ω_q, and γ_q.

To acquire an IVSFG spectrum, the *nc*-Si/MS samples were simultaneously excited by 20 ps (1 ps $= 1 \times 10^{-12}$ s) optical pulses at $\lambda = 532$ nm and infrared pulses with a tunable wavelength between 3.5 and 7 μm. The reflected optical SFG signal with wavelength near 480 nm was recorded as a function of the infrared frequency. The measured IVSFG spectra of MS (dashed curve) and as-grown *nc*-Si/MS film (lines with symbols) are shown in Figure 4a. Broad resonance was detected as the infrared frequency was tuned from 2 300 to 1 800 cm^{-1}. We can attribute the complicated resonances to be either from Si−H ($\omega_{Si-H} \approx 2\,100\ cm^{-1}$) stretching[15] or the overtone of Si=O stretching ($2\omega_{Si=H} \approx 2\,100\ cm^{-1}$).[16] Si=O double bonds are likely to be formed and stabilize the interfaces of *nc*-Si and MS matrix, since the formation of Si=O requires neither a large deformation energy nor an excess element. The broad resonance indicates that the bonding geometry is complex at the interfaces of *nc*-Si and MS.[17,18] Furthermore, the *s*-polarized SFG signal is weaker than the *p*-polarized signal, suggesting the polar bonding structure to be more or less normal to the film surface.

$LiNbO_3$ is a ferroelectric crystal with a polar unit cell structure and can be used as a convenient reference. By comparing the reflected IVSFG signal from the as-grown *nc*-Si/MS film to that from a *z*-cut $LiNbO_3$ plate under the same excitation level and beam geometry, we estimated the resonant IVSFG susceptibility of the *nc*-Si/MS film to be $\chi_{s,ppp}^{(2)} = 7.6\ pm \cdot V^{-1}$. The IVSFG susceptibility is about the averaged value of the second-order nonlinear optical responses of ferroelectric crystals and cannot originate from an isotropic film with much weaker quadrupoles.[19] Therefore, a one-side bonding picture from preferential growth of *nc*-Si on the bottom of the pore-channels is proposed (Fig. 4b).

As shown in Figure 1b, the number density of *nc*-Si in MS is about $N_p = 2.5 \times 10^{18}\ cm^{-3}$. The number density of Si atoms in SiO_2 is known to be $2.3 \times 10^{22}\ cm^{-3}$, implying that the surface density of Si atoms in a 1 nm thick interfacial layer between Si and SiO_2 is about $2.3 \times 10^{15}\ cm^{-2}$. Therefore, there are about $N_b = 300$ heteropolar bonds in the hemispherical interface of a 4 nm diameter one-side-bonded Si nanocrystal. By using $\chi^{(2)} = N_p N_b \langle\alpha^{(2)}\rangle / \varepsilon_0$, with $\langle\alpha^{(2)}\rangle$ being the SF molecular polarizability and ε_0 the permittivity of free space, we estimated $\langle\alpha^{(2)}\rangle = 9.0 \times 10^{-50}\ m^3 C V^{-2}$ for each heteropolar bond from the measured SF susceptibility. The measured $\langle\alpha^{(2)}\rangle$ has a similar value to that of C−H stretching on the surface of a poly(vinyl alcohol) film,[20] affirming the polar bonding nature at the interfaces of *nc*-Si/MS.

The polar structure of the interfacial bonds in *nc*-Si/MS should yield a nonvanishing electric polarization, the direction of which should be switchable by using an electric field to displace the centers of gravity of the positive and negative charge distributions. To verify this, we fabricated a metal-insulator-metal (MIM) capacitor with a 400 μm diameter top aluminium pad. The electrical polarization in the insulation stack comprising of a 90 nm thick *nc*-Si/MS film was monitored with polarization-electric field (P-E) measurements[21] and the results are presented in Figure 4c. The hysteresis loop is not closed due to a small current leakage occurring in the device under test. The remnant polarization $\boldsymbol{P}_r$ of the sample was found to be 5 μC cm^{-2}, which is much larger than the reported values for iron-passivated

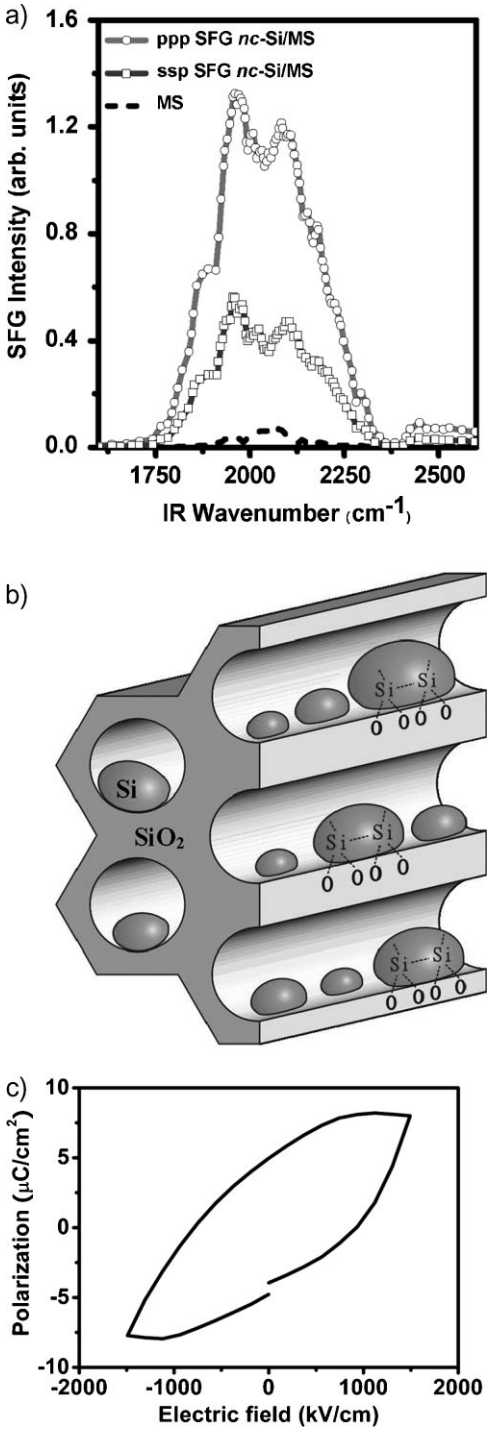

Figure 4. Experimental characterization for the polar bonding structure of *nc*-Si/MS. a) The sum-frequency signal from MS (dashed line) and as-grown *nc*-Si/MS layer (symbols) are presented as a function of infrared frequency. Here *ppp* (open circles) and *ssp* (open squares) denote the beam polarization directions (from left to right) of the sum-frequency beam at 480 nm, the visible-beam at 532 nm and the infrared beam to be either *p*-polarized (lying on the incident plane) or *s*-polarized (perpendicular to the incident plane). b) Schematic drawing illustrating the one-side bonding geometry of Si nanocrystals. c) The polarization-electric field hysteresis of a metal-(*nc*-Si/MS)-metal capacitor device.

porous silicon.[22] By using the known number density of *nc*-Si in MS, the measured remnant polarization indicates each one-side bonded Si nanocrystal to have an averaged dipole moment of 2×10^{-18} μC cm.

In addition to the experimental results shown above, a theoretical study[23] has indicated that both the Si atoms in the nanocrystals and the O atoms at the interface are crucial for determining the optical properties of *nc*-Si/MS. To further study the nature of induced optical polarization in this nanostructured material, an as-grown *nc*-Si/MS film was prepared and excited by

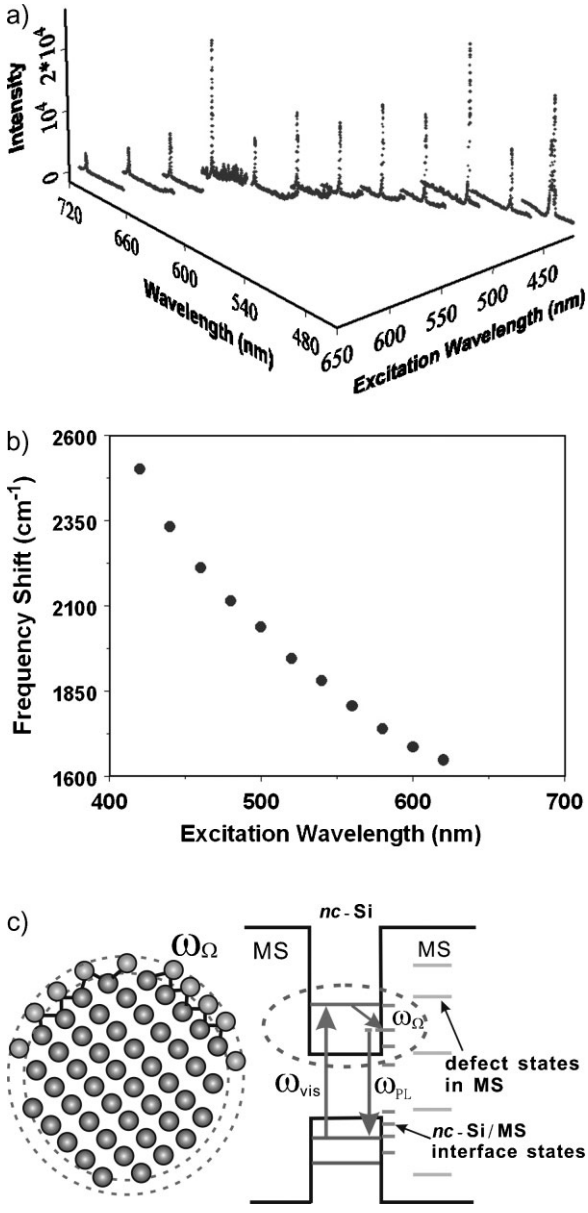

Figure 5. Optical emission spectra of *nc*-Si/MS. a) Optical emission spectra at room temperature from an as-grown *nc*-Si/MS film excited by 20 ps optical pulses presented as a function of the excitation wavelength from 400 to 700 nm. b) The energy interval between the energy of excitation and peak emission is presented as a function of the excitation wavelength. c) Energy-level diagram illustrating the optical emission process.

20 ps optical pulses tunable between 400 and 700 nm; the resulting optical emission spectra are presented in Figure 5a. The optical emission peak was found to shift to higher energy with increasing excitation energy and exhibits a very narrow bandwidth. This phenomenon had never been observed on any quantum dot system at room temperature. The energy interval Δ_{st} between the energy of excitation and peak emission (Fig. 5b) is much larger than the reported 57 meV ($\sim$456 cm^{-1}) of TO phonons in crystalline silicon.[24] Recent transient photo-induced absorption measurements by Lioudakis, et al.[25] suggest that the light-absorption process takes place inside the *nc*-Si band structure, and the photoexcited carriers related to PL are in oxygen-related states. The photoexcited carriers in the oxygen-related interface states couple strongly with quantized sublevels of *nc*-Si, resulting in ultrafast relaxation of the photoexcited carriers. A coupling effect of carriers with the stretch mode of interfacial species has also been reported in other quantum dot systems.[26] Based on these findings, our optical emission measurements can therefore be interpreted with the schematic shown in Fig. 5c. The large Δ_{st} is caused by interactions between carriers and stretch vibrations of interfacial species. Only the photoexcited electrons in the Si quantum dots with correct diameter, labeled by the excitation wavelength, can resonantly couple to the stretch vibration of interfacial species and results in the observed Stokes-shifted optical emission. For incident photons in the near-infrared region, optical transitions can occur from occupied to unoccupied interface states. Since the numbers of atoms on the surface and in the bulk of *nc*-Si/MS are comparable, significant optical response from the interface states is expected in the near-infrared region.

The carrier-phonon coupling strength can increase with localization of carriers in smaller dimensions, since the higher the charge density of the captured electron, the greater the force on the nearby ions and hence the larger the coupling strength.[27] To estimate the localization effect of a photo-excited carrier, we assume the *nc*-Si to have a radius of r capped with an electric polarization shell of thickness δr, which contains $\boldsymbol{N}_{\mathbf{b}}$ radially pointing electric dipoles $\boldsymbol{\mu}$. The *nc*-Si has a high-frequency dielectric constant ε_∞ and static dielectric constantε_s, resulting in an impermittivity difference of $\Delta[1/\bar{\varepsilon}] = [1/\varepsilon_\infty] - [1/\varepsilon_s]$. Assuming that the carrier is confined within the shell, the electron-phonon interaction energy H_{ep} can be estimated with:

$$H_{ep} = e(N_b\mu)\Delta[1/\bar{\varepsilon}]/(4\pi\varepsilon_0 r^2) \quad (2)$$

The electron-phonon coupling strength can be revealed with the Huang–Rhys factor $S = |H_{ep}|/\hbar\omega_v$,[28] giving the average number of phonons involved per photon emission. By using $N_b\mu = 2\times10^{-26} C\cdot m$, $\Delta[1/\bar{\varepsilon}] \approx 0.02$, $\hbar\omega_v = 2000\ cm^{-1} = 248$ meV, and $r = 2$ nm, we obtained $S_{sh} \approx 3.6$. When the carrier is distributed uniformly inside the quantum dot with a shell thickness of $\delta r = 1\ nm$, S is moderately reduced to $S_{dot} = 3S_{sh}r^2\delta r/2(r+\delta r)^3 \approx 0.8$. Strong coupling between interfacial optical phonons and photoexcited carriers is thus expected in *nc*-Si/MS.

Small values of S for interband transitions in the bulk crystal are usually due to there being nearly identical distributions of the electron and hole wave-functions, which causes near cancellation of their contributions to the diagonal matrix element of the electron-phonon interaction. One may expect larger S values for the intraband transition because of a large difference in the symmetry of the initial and final states involved.[29] The one-sided-bonding model shown in Figure 4b results in a non-zero diagonal matrix element of the electron-phonon interaction, since this geometry breaks the spherical symmetry of the charge distribution. Furthermore, non-adiabatic electron-phonon interaction can also occur, in which the electron motion is coupled to the ion motion in the crystal Hamiltonian. Strong localization of the wave-functions in quantum dots under non-adiabatic condition has been shown to be efficient for phonon emission, yielding a larger Huang-Rhys parameter than for bulk materials.[30]

A scenario was proposed to explain the enhanced photo-responsivity shown in Figure 2. The absorption process of incoming photons in the visible region first takes place inside the *nc*-Si band structure. Depending on the wavelength of the incident photons, only photoexcited electrons in the Si quantum dots with the correct diameter can efficiently tunnel to the defect states in MS, mediated by a resonant coupling with the stretch vibration of interfacial species. Since the mechanism depends on the excitation of electrons in Si quantum dots of the right diameter, the polydispersity of *nc*-Si shown in Figure 1b may limit the efficiency of the material. However, we emphasize that the polydispersity of Si quantum dots also yields the advantage of an extended optical response range due to the size-dependent quantum-confined effect.

3. Conclusions

We report a new class of artificially engineered optoelectronic materials formed by embedding three-dimensional arrays of *nc*-Si (or *nc*-Ge) in a mesoporous silica matrix. The resulting photoresponsivity was improved beyond that of silicon crystal. Material characterizations showed that the nanocrystals form highly stable one-side-bonded interface structures and yield significant dipolar effect. The polar structures, verified by infrared-visible sum frequency vibrational spectroscopy, possess a resonant second-order nonlinear susceptibility of 7.6 pm V^{-1} and exhibit a ferroelectric-like hysteresis. A design concept that employs semiconductor nanocrystals for optical sensing and utilizes interfacial polar layers to facilitate the carrier transport and emulate a ferroelectric-like switching was verified. This new class of artificially engineered multifunctional materials promises better performances in various applications, ranging from photon detection, photovoltaic conversion, to nonvolatile memory devices.

4. Experimental

Preparation of Mesoporous Silica Nanotemplate: An MS nanotemplate layer was prepared by spin coating on *n*- or *p*-type silicon substrate. To prepare the spin-coating solution, we first produced an acid-catalyzed silica sol-gel by refluxing a mixture of tetraethylorthosilicate (TEOS), triblock copolymer Pluronic P-123 (P123), H_2O, HCl and ethanol with a molar ratio of 1:0.008–0.03:3.5–5.0:0.003–0.03:40 at 60–80 °C for 60–120 min. A precursor solution was then made by adding an ethanol solution of P123 to the acid-catalyzed silica sol-gel. After the precursor solution was aged at room temperature for 3–6 h at ambient conditions, it was spin-coated onto the substrates at 3 000 rpm for 30 s. The film was dried at 40–60 °C for

4–6 h, and then baked at 100–120 °C for 3 h. The resulting mesoporous silica film was used as the nanotemplate to synthesize Si nanocrystals (*nc*-Si).

In Situ Synthesis of Si Nanocrystals: *nc*-Si was grown with an inductively coupled plasma chemical vapor deposition (ICPCVD) system. The apparatus can be controlled at a level of clusters with a base pressure of 10^{-6} torr. The plasma was formed by sequentially exciting a mixture of (SiH_4 + H_2) or pure H_2 with a radio-frequency (RF) electrical power of 500 W. The gas pressure was kept below 10 mtorr and the substrate temperature maintained at 250 °C during the growth process. Similar to the typical gap-filling/etching process used in integrated circuit manufacturing to yield an enhanced anisotropic etching effect, the substrates were electrically biased. This was achieved by applying an electrical power of 300 W at 300 kHz on the substrate to create a condition for preferential growth of *nc*-Si on the bottom of the pore-channels. The formation of high-quality *nc*-Si involves several critical steps. First, the pure H_2 ICP was used to remove small areas of the organic templates of MS to form nucleation sites of Si—OH on the surfaces of pore channels. The nucleation sites are important for a self-limiting growth reaction (SLR), which is the key for atomic layer deposition. Subsequently, ICP-excited SiH_n species in the form of nanoclusters diffused into the pore channels of MS, and then absorbed on the pore surfaces. The adsorbed species eventually reacted with the nucleation sites of Si—OH via a hydrogen-elimination reaction (HER). SLR, in cooperation with HER, precisely governs the conversion of ICP-excited species bound in MS into *nc*-Si. The number density of *nc*-Si grown by pulsed plasma can be as high as 2.5×10^{18} cm^{-3}, which is about 5–10 times higher than that grown by steady-state plasma, where only HER is involved during the growth of *nc*-Si. The organic contents of MS can be removed in situ by calcination with H_2 plasma at a flow rate of 200 sccm for 10 min. For device applications, a 10 nm thick SiO_2 film was deposited with ICP CVD on an *nc*-Si/MS film. Since all sample preparation processes were conducted sequentially in the high-vacuum environment, the quality and characteristics of the interfaces between *nc*-Si and MS matrix can be accurately controlled and be reproducible.

Electrical Characterization: The P-E characteristics of *nc*-Si/MS film were analyzed by using a Metal-Insulator-Semiconductor (MIS) structure. The testing devices involve an insulation (I) stack of SiO_2 (10 nm)/*nc*-Si/MS (90 nm)/SiO_2 (10 nm) stack. The top electrode pad of the device was made of an aluminium film with 400 μm diameter and the back-side of the semiconductor substrate (S) was coated with a blanket aluminium film. The P-E of a MIS device with pure MS film does not exhibit detectable hysteresis.

Acknowledgements

J. Y. Huang and C. L. Pan acknowledge funding by the National Science Council (NSC), through PPAEU-II and other grants, and the Academic Top Universities (ATU) program of the Ministry of Education.

Received: September 9, 2008
Revised: December 16, 2008
Published online:

[1] C. V. Cojocaru, F. Ratto, C. Harnagea, A. Pignolet, F. Rosei, *Microelectron. Eng.* **2005**, *80*, 448.
[2] C. H. Ahn, K. M. Rabe, J.-M. Triscone, *Science* **2004**, *303*, 488.
[3] H. Yamada, Y. Ogawa, Y. Ishii, H. Sato, M. Kawasaki, H. Akoh, Y. Tokura, *Science* **2004**, *305*, 646.
[4] M. Galperin, M. A. Ratner, A. Nitzan, A. Troisi, *Science* **2008**, *319*, 1056.
[5] S. Tiwari, F. Rana, H. Hanafi, A. Hartstein, E. F. Crabbe, K. Chan, *Appl. Phys. Lett.* **1996**, *68*, 1377.
[6] G. R. Lin, C. J. Lin, H. C. Kuo, *Appl. Phys. Lett.* **2007**, *91*, 093122.
[7] H. Y. Fan, K. Yang, D. M. Boye, T. Sigmon, K. J. Malloy, H. F. Xu, G. P. López, C. J. Brinker, *Science* **2004**, *304*, 567.
[8] A. T. Cho, J. M. Shieh, J. Shieh, Y. F. Lai, B. T. Dai, F. M. Pan, H. C. Ku, Y. C. Lin, K. J. Chao, P. H. Liu, *Electrochem. Solid-State Lett.* **2005**, *8*, G143.
[9] J. M. Shieh, Y. F. Lai, W. X. Ni, H. C. Kuo, C. Y. Fang, J. Y. Huang, C. L. Pan, *Appl. Phys. Lett.* **2007**, *90*, 051105.
[10] M. K. Lee, C. H. Chu, Y. H. Wang, S. M. Sze, *Opt. Lett.* **2001**, *26*, 160.
[11] J. Y. Zhang, X. M. Bao, Y. H. Ye, X. L. Tan, *Appl. Phys. Lett.* **1998**, *73*, 1790.
[12] M. V. Wolkin, J. Jorne, P. M. Fauchet, G. Allan, C. Delerue, *Phys. Rev. Lett.* **1999**, *82*, 197.
[13] T. Baron, B. Pelissier, L. Perniola, F. Mazen, J. M. Hartmann, G. Rolland, *Appl. Phys. Lett.* **2003**, *83*, 1444.
[14] J. Y. Huang, Y. R. Shen, in *Laser Spectroscopy and Photochemistry on Metal Surfaces, Adv. Ser. Phys. Chem.*, Vol. 5(Eds: H. L. Dai, W. Ho), Wiley, New York, USA **2003**, Ch. 1.
[15] A. H. M. Smets, M. C. M. van de Sanden, *Phys. Rev. B* **2007**, *76*, 073202.
[16] A. Sa'ar, Y. Reichman, M. Dovrat, D. Krapf, J. Jedrzejewski, I. Balberg, *Nano Lett.* **2005**, *5*, 2443.
[17] M. V. Wolkin, J. Jorne, P. M. Fauchet, G. Allan, C. Delerue, *Phys. Rev. Lett.* **1999**, *82*, 197.
[18] A. Puzder, A. J. Williamson, J. C. Grossman, G. Galli, *Phys. Rev. Lett.* **2002**, *88*, 097401.
[19] P. Figliozzi, L. Sun, Y. Jiang, N. Matlis, B. Mattern, M. C. Downer, S. P. Withrow, C. W. White, W. L. Mochan, B. S. Mendoza, *Phys. Rev. Lett.* **2005**, *94*, 047401.
[20] X. Wei, X. Zhuang, S. C. Hong, T. Goto, Y. R. Shen, *Phys. Rev. Lett.* **1999**, *82*, 4256.
[21] K. J. Choi, M. Biegalski, Y. L. Li, A. Sharan, J. Schubert, R. Uecker, P. Reiche, Y. B. Chen, X. Q. Pan, V. Gopalan, L. Q. Chen, D. G. Schlom, C. B. Eom, *Science* **2004**, *306*, 1005.
[22] Q. Chen, X. Li, Y. Zhang, Y. Qian, *Adv. Mater.* **2002**, *14*, 134.
[23] N. Daldosso, M. Luppi, S. Ossicini, E. Degoli, R. Magri, G. Dalba, P. Fornasini, R. Grisenti, F. Rocca, L. Pavesi, S. Boninelli, F. Priolo, C. Spinella, F. Iacona, *Phys. Rev. B* **2003**, *68*, 085327.
[24] I. Sychugov, R. Juhasz, J. Valenta, J. Linnros, *Phys. Rev. Lett.* **2005**, *94*, 087405.
[25] E. Lioudakis, A. Othonos, A. G. Nassiopoulou, *Appl. Phys. Lett.* **2007**, *90*, 171103.
[26] P. Guyot-Sionnest, B. Wehrenberg, D. Yu, *J. Chem. Phys.* **2005**, *123*, 074709.
[27] J. Martin, F. Cichos, F. Huisken, C. von Borczyskowski, *Nano Lett.* **2008**, *8*, 656.
[28] L. Jacak, J. Krasnyj, W. Jacak, *Phys. Lett. A* **2002**, *304*, 168.
[29] J. Kundrotas, A. C. Erškus, S. Ašmontas, G. Valušis, M. P. Halsall, E. Johannessen, P. Harrison, *Semicond. Sci. Technol.* **2007**, *22*, 1070.
[30] S. Menzel, E. A. Zibik, P. Aivaliotis, J. W. Cockburn, L. R. Wilson, M. J. Steer, *Phys. Rev. B* **2008**, *77*, 153302.